JACS
JOURNAL OF THE AMERICAN CHEMICAL SOCIETY

ARTICLE

pubs.acs.org/JACS

A New Aluminosilicate Molecular Sieve with a System of Pores between Those of ZSM-5 and Beta Zeolite

Manuel Moliner,[†] Jorge González,[†,‡] M. Teresa Portilla,[†] Tom Willhammar,[∥] Fernando Rey,[†] Francisco J. Llopis,[§] Xiaodong Zou,[∥] and Avelino Corma*[,†]

[†]Instituto de Tecnología Química (UPV-CSIC), Universidad Politécnica de Valencia, Consejo Superior de Investigaciones Científicas, Valencia 46022, Spain

[‡]Escuela de Ciencias Químicas, Universidad de Colima, Colima 28040, Mexico

[§]Departamento de Ingeniería Química, Universitat de Valencia, Burjassot 46100, Spain

[∥]Berzelii Centre EXSELENT on Porous Materials and Inorganic and Structural Chemistry, Department of Materials and Environmental Chemistry, Stockholm University, SE-106 91 Stockholm, Sweden

Supporting Information

ABSTRACT: A new aluminosilicate zeolite (ITQ-39) has been synthesized. This is an extensively faulted structure with very small domains that makes the structure elucidation very difficult. However, a combination of adsorption spectroscopy and reactivity studies with selected probe molecules suggests that the pore structure of ITQ-39 is related to that of Beta zeolite, with a three-directional channel system with large pores (12-MR), but with an effective pore diameter between those of Beta and ZSM-5, or a three-directional channel system with interconnected large (12-MR) and medium pores (10-MR). The pore topology of ITQ-39 is very attractive for catalysis and shows excellent results for the preparation of cumene by alkylation of benzene, while it can be a promising additive for FCC.

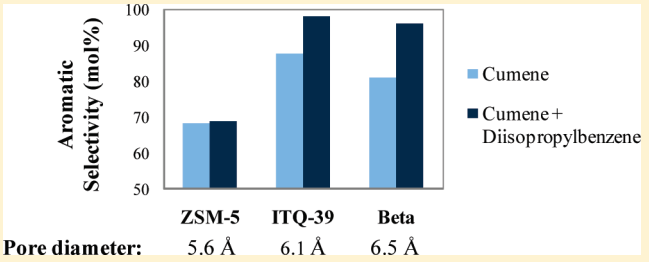

1. INTRODUCTION

Zeolites are crystalline microporous materials frameworks formed by T atoms (primarily Si and Al) in tetrahedral coordination that generate three-dimensional structures defined by pores and cavities of molecular dimensions.[1] The manufacture of zeolites in the laboratory mimicking the hydrothermal conditions found in nature, together with the introduction of organic molecules acting as pore filling agents, has allowed the production of zeolites with different pore architectures.[2] As a consequence, the scientific interest on those structures has been increasing, together with their industrial applications (catalysis, adsorbents, ion exchangers, medicine, electronics, etc.).[3]

Nowadays, there are more than 190 different zeolite framework types accepted by the International Zeolite Association (IZA),[4] which are classified according to the channel system (monodirectional, bidirectional, or three-directional) or to the pore size (small-8-MR, medium-10-MR, large-12-MR, or extra-large-12-MR). It has to be remarked the important number of extra-large pore zeolites and zeolitic materials that have been discovered in the last 5 years, some of them with chiral frameworks, combining the structure-directing effect of framework inorganic cations other than Si and Al, with the directing role of organic molecules.[5] Despite the large number of already existing zeolites, the discovery of a new structure with unique textural properties or different chemical composition is always an interesting challenge, and relevant work combining computer modeling synthesis and structure determination has been published recently.[6]

The search for applications of a new zeolite is guided by its structure. However, the structure elucidation can be sometimes difficult, because of its complexity, the small size of the crystals, or the presence of defects or impurities.[7] A paradigmatic example was the case of Beta zeolite,[8] the structure of which remained unresolved for more than 20 years.[9] This was due the fact that Beta zeolite is formed by stacking sequences of two polymorphs (A and B) that coexist in small domains in the same crystal. The presence of those small areas of each polymorph causes broadening of the peaks in the powder X-ray diffraction, increasing the reflection overlapping.[10] The structure of Beta zeolite was elucidated by a combination of high-resolution electron microscopy, electron diffraction, and computer-assisted modeling.[9] Recently, other complex structures, such as TNU-9,[11a] IM-5,[11b] SSZ-74,[11c] and ITQ-37,[5a] have been solved by combination of selected area electron diffraction (SAED) patterns, high resolution transmission electron microscopy (HRTEM) images, and powder X-ray diffraction. Zeolite Beta polymorph B and IM-5 could be solved from SAED patterns

Received: March 4, 2011
Published: May 18, 2011

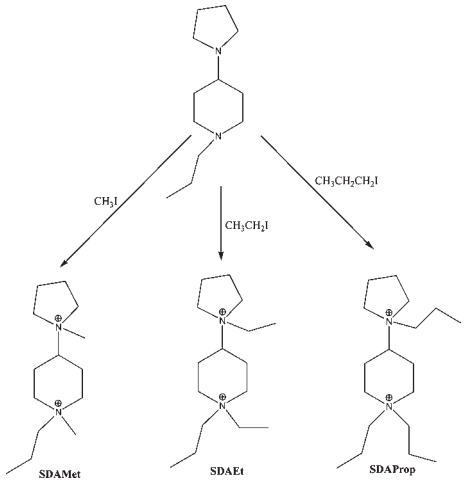

Figure 1. Organic structure-directing agents used for the ITQ-39 synthesis.

and HRTEM images combined with crystallographic image processing.[12]

Despite the advances described in the structure elucidation of new materials, there are occasions where the achievement of the real structure is still a complex problem. This is the case of the molecular sieve described here, named ITQ-39.[13] In this situation, one may get inside the pore topology and pore dimensions by considering that the selectivity toward a desired product in a chemical process will change depending on the shape and size of the channels of the zeolite. Next, the combination of adsorption and reactivity of selected probe molecules can provide a good approximation to the pore topology,[14] and from this, to predict its possibilities for the different industrially relevant catalytic processes.[15]

Here, we will present the synthesis procedure and the characterization of a new zeolite, named ITQ-39. This molecular sieve shows an extensively faulted structure, making the structure elucidation very difficult. For this reason, we will use a combination of characterization techniques, and a series of catalytic test reactions, to approximate the pore structure of ITQ-39. Further knowledge is gained by comparing its catalytic behavior with other two zeolites, one medium pore size (ZSM-5) and one large pore size (Beta).

2. EXPERIMENTAL SECTION

2.1. Organic Structure-Directing Agent (OSDA) Synthesis. The OSDA cation was prepared as follows: 30 g of pyrrolidine (Sigma-Aldrich, 99%) was dissolved in 200 mL of methanol (Sigma-Aldrich, >99%). The solution was acidified with HCl (Fluka, 5 N in methanol) until pH = 7.5, and then the mixture was cooled continuously at 273 K. Next, 37 g of 1-propyl-4-piperidone (Sigma-Aldrich, 99%) was added, followed by 10.5 g of sodium cyanoborohydride ($NaBH_3CN$, Fluka, >95%). The resultant mixture was stirred during 72 h at room temperature.

After that, HCl was added slowly until reaching a pH close to 2, with the HCN being removed by nitrogen flow. The solution was concentrated, and then a KOH solution was added until arriving to pH > 12. In this case, a white precipitate was obtained. The mixture was saturated with NaCl. Finally, the diamine 1-propyl-4-pyrrolidin-1-yl-piperidine was extracted with diethyl ether and dried with anhydrous $MgSO_4$.

The quaternization of diamine was done as follows: over 20 g of diamine solution in 70 mL of MeOH was added 60 g of alkyl iodide (methyl, ethyl, or propyl; see Figure 1). After 7 days under stirring at room temperature, a white precipitate was obtained, which was filtered and washed with methanol and diethyl ether. Finally, the solid was dried under high vacuum.

Table 1. Synthesis Conditions and Zeolites Obtained by Using SDAProp during t = 14 days as Crystallization Time

T (K)	Si/Al = ∞	Si/Al = 50	Si/Al = 25	Si/Al = 13	Si/Al = 7
408	ZSM-5	ZSM-5	ITQ-39	ITQ-39	ITQ-39
423	ZSM-5	ZSM-5	ITQ-39-ZSM-5	ITQ-39	ITQ-39
448	ZSM-5	ZSM-5	ZSM-5	ZSM-5	ZSM-5

The iodide form of the organic salt was exchanged to the hydroxide form as follows: 44 mmol of cation in the iodide form was dissolved in water, and 89 g of resin Dower SBR was added, maintaining under agitation overnight. The solution was filtered, and the dihydroxide cation was obtained.

2.2. Zeolite Synthesis. The general synthesis procedure was as follows: aluminum isopropoxide (Sigma-Aldrich, >98%) was added over tetraethylorthosilicate (TEOS, Sigma-Aldrich, >99%). Next, a solution of $OSDA(OH)_2$ was added. The mixture was stirred until complete hydrolysis of the TEOS, and then allowed to reach the desired water ratio by complete evaporation of ethanol and some water. Finally, an HF solution (Merck, 48 wt%) was dosed, obtaining the final gel composition: SiO_2:0−0.07Al_2O_3:0.25$OSDA(OH)_2$:0.50HF:2.5H_2O, where OSDA is one of the dicationic molecules described in the previous paragraph. For the synthesis of pure silica samples, some seeds of ITQ-39 crystals (8 wt %) were added to the synthesis gel.

The gel was heated during the required time (see Tables 1 and 4) in a steel autoclave with a Teflon lined vessel, at 408−448 K in static conditions. The final powder after filtration and washing with distilled water was ITQ-39.

ZSM-5 (TZP322) and Beta (PQ13) were supplied by Tricat GmbH and Zeolyst International, respectively. The supplied samples in their ammonic form were calcined at 773 K during 3 h to obtain the acid zeolites.

2.3. Characterization. Synthesized samples were characterized by powder XRD using a multisample Philips X'Pert diffractometer equipped with a graphite monochromator, operating at 40 kV and 45 mA, and using Cu K_α radiation (λ = 0.1542 nm).

The chemical analysis was performed in a 715-ES ICP-Optical Emission spectrometer, after solid dissolution in HNO_3/HCl/HF aqueous solution. The organic content of the as-made materials was determined by elemental analysis performed on a SCHN FISONS elemental analyzer.

The morphology of the samples was studied by scanning electron microscopy (SEM) using a JEOL JSM-6300 microscope.

The SAED patterns were collected on a JEOL 2100F transmission electron microscope at 200 kV. Samples for TEM were grounded and dispersed in ethanol by ultrasound. A drop of the suspension was transferred onto a copper grid covered by holey carbon films. SAED patterns were collected on a Gatan Ultrascan 1000 CCD camera. The d-values of reflections were obtained from the SAED patterns using the program ELD.[16]

Textural properties were determined by Ar and N_2 adsorption−desorption isotherms measured on a Micromeritics ASAP 2020 at 87 and 77 K, respectively.

NMR spectra of solids were recorded at room temperature under magic angle spinning (MAS) in a Bruker AV-400 spectrometer. ^{19}F was measured at 376.28 MHz using a Bruker probe with 2.5 mm diameter zirconia rotors spinning at 25 kHz. The ^{19}F spectra were collected using pulses of 4.5 μs corresponding to a flip angle of $\pi/2$ rad, and a recycle delay of 100 s to ensure the complete recovery of the magnetization. The single pulse ^{29}Si spectra were acquired at 79.5 MHz with a 7 mm Bruker

Table 2. Elemental, Chemical, and Thermo-gravimetric Analysis for ITQ-39 Samples with Different Si/Al Ratios

Si/Al_{teor} [a]	Si/Al_{real} [b]	OSDA	N (wt %)	C (wt %)	H (wt %)	C/N	TGA (wt %)
7	9.5	SDAProp	1.92	14.90	2.71	9.05	23
10	11.5	SDAProp	1.78	13.80	2.40	9.06	22
13	12.9	SDAProp	1.87	14.67	2.71	9.15	23
25	22.1	SDAProp	1.86	14.21	2.62	8.92	22
INF	INF	SDAEt	1.99	14.02	2.52	8.20	23

[a] Si/Al ratio in the synthesis gel. [b] Si/Al ratio in the final solid.

BL-7 probe using pulses of 3.5 μs corresponding to a flip angle of 3/4 π radians, and a recycle delay of 60 s.

The relative concentration of acidic sites in the different samples was obtained by FT-IR spectroscopy using pyridine as the probe molecule. Pyridine adsorption−desorption experiments were carried out on self-supported wafers (10 mg cm^{-1}) activated at 673 K and 10^{-2} Pa for 2 h. After sample activation, pyridine vapor (6.5×10^2 Pa) was admitted into the vacuum IR cell and adsorbed onto the zeolite at room temperature. Desorption was performed in a vacuum over three consecutive 1 h periods of heating at 423, 523, and 623 K, each followed by an IR measurement at room temperature. All of the spectra were scaled according to the sample weight.

2.4. Catalytic Tests. Catalytic experiments were conducted in vapor phase at atmospheric pressure in a fixed bed continuous glass down-flow reactor (11 mm internal diameter).[15a] The *meta*-xylene isomerization was carried out with a N_2/*meta*-xylene molar ratio of 4. For alkylation reactions, the aromatic compound was fed in excess to the alcohol, with a molar ratio aromatic/alcohol of 4. N_2 was used as carrier gas with N_2/alcohol molar ratio of 10. Before the addition of reactants, the catalyst was treated within the reactor at 623 K with a heating program of 5 K/min under nitrogen flow. After 30 min, the temperature was raised to 723 K kept for 1 h. The reactor was then cooled to reaction temperature, 623 K for *meta*-xylene isomerization or 553 K for benzene or toluene alkylation. The products of the reactions were analyzed by gas chromatography (HP5890II, equipped with a TR-WAX-10 capillary column, 60 m length, inner diameter 0.2 mm) and a flame ionization detector (FID).

3. RESULTS AND DISCUSSION

3.1. Synthesis and Characterization. The phase diagram obtained using SDAProp (see Figure 1) as OSDA is summarized in Table 1. There, it is shown the crystallization of a known material (ZSM-5), together with an unknown structure, named ITQ-39 zeolite. ITQ-39 crystallizes at low temperatures (408 and 423 K) and large content of aluminum in the synthesis media (Si/Al < 25), while ZSM-5 was the preferred phase when the temperature is increased or the aluminum removed from the synthesis gel.

As it can be seen in Table 2, elemental analyses show that the organic SDAProp is intact in the as-prepared ITQ-39 samples (C/N ratio 9), and the total organic amount being confined in the inorganic framework is close to 22 wt % (calculated by thermo-gravimetric analysis). Moreover, the scanning electron microscopy (SEM) image of the powder (see Figure 2) reveals that the ITQ-39 sample is formed by aggregation of very small crystals (~100−150 nm).

The powder XRD patterns of the as-prepared and calcined forms of ITQ-39 are presented in Figure 3. The diffractogram comprises both sharp and broad peaks, which is indicative of an extensively faulted structure. Because in a very first approximation the diffractogram of ITQ-39 reminds us of that of Beta, the

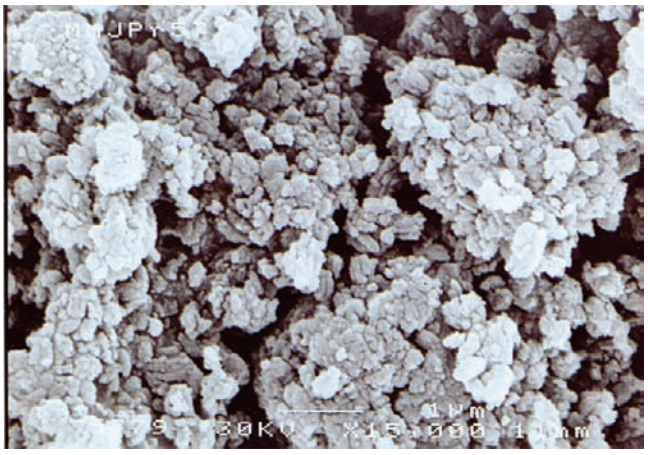

Figure 2. Scanning electron microscopy (SEM) image of the ITQ-39 zeolite.

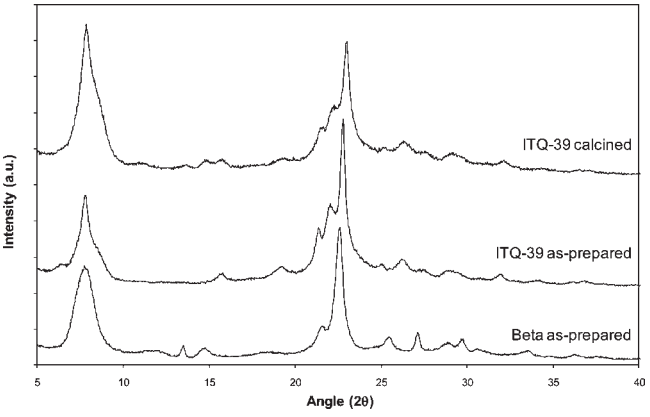

Figure 3. Powder XRD patterns for the as-prepared ITQ-39, calcined ITQ-39, and as-prepared Beta zeolite.

XRD patterns of ITQ-39 and Beta zeolite are compared in Figure 3. The results indicate certain similarities between them, but also significant differences. The principal differences between both diffractograms, among others, are the presence in the ITQ-39 of a peak in the 2θ angle close to 6.5°, a peak at 7.5° that shows a pronounced shoulder, and three consecutive peaks between 21° and 23°.

As it has been described before, Beta zeolite is formed by an intergrowth of two different polymorphs with stacking disorder,[9] and, from the related diffractogram profile, ITQ-39 could present similar disorder with large number of defects. As it can be seen in Figure 4, selected area electron diffraction patterns (SAED) show that ITQ-39 exhibits disorder similar to that of zeolite Beta. Similar diffuse lines along the c^*-axis for reflections $h0l$ with $h \neq 3n$ in zeolite Beta are observed in ITQ-39. This indicates that the stacking disorder in ITQ-39 is similar to that of Beta. Assuming that the unit cell setting for ITQ-39 is chosen in the same way as for Beta polymorph A ($a = b = 12.85$ Å, $c = 13.56$ Å) (see Figure 4), the d_{100}-value (=$1/a^*$) of ITQ-39 is 12.77 Å, similar to that of Beta (12.85 Å), while the d_{001}-value (=$1/c^*$) of ITQ-39 is 11.45 Å, 2.11 Å smaller than the corresponding d-value of Beta (13.56 Å). From the TEM study, we can conclude that the structures of ITQ-39 and Beta have some similarities, with the c-axis in ITQ-39 being significantly shorter than that in Beta.

dx.doi.org/10.1021/ja2015394 |*J. Am. Chem. Soc.* 2011, 133, 9497–9505

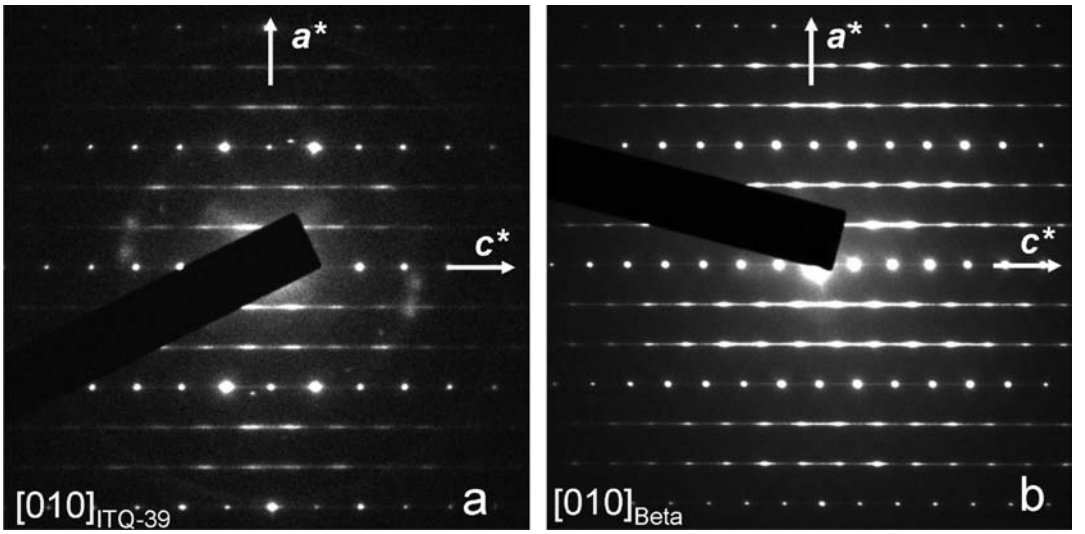

Figure 4. Selected area electron diffraction patterns (SAED) taken from (a) ITQ-39 and (b) zeolite beta. The unit cell settings are chosen according to the Beta polymorph A.

Table 3. Textural Properties of the ZSM-5, ITQ-39, and Beta Zeolite by Means of Adsorption of N_2 and Ar

zeolite	BET area (m^2/g)	micropore area (m^2/g)	micropore volume (cm^3/g)	pore diameter (Å)	topology
ZSM-5	379	320	0.15	5.6	2D-10MR
ITQ-39	547	352	0.17	6.1	
Beta	586	420	0.21	6.5	3D-12MR

N_2 and Ar adsorption have been carried out with ITQ-39, Beta, and ZSM-5, and the textural properties of those three materials are summarized in Table 3. The micropore volumes obtained from N_2 adsorption reveal that the value for ITQ-39 lies between Beta and ZSM-5. Furthermore, the Ar adsorption indicates that the pore diameter of ITQ-39 obtained with the Horvath−Kawazoe formalism[17] is intermediate between the pore diameter of Beta and ZSM-5 (see also Figure 5). Both achieved values for the micropore volume and pore diameter for the ITQ-39 agree with a possible three-directional large pore zeolite with an effective pore diameter between those of Beta and ZSM-5 zeolite, or a three-directional pore system with interconnected large and medium pores. However, we cannot see in Figure 5 a clear indication of the existence of medium and large pores in the structure as it would be indicated by the presence of two peaks in Figure 5, as it occurs, for instance, in the case of the recently synthesized Boggsite.[18]

Pure silica ITQ-39 zeolite was synthesized to obtain more information about its structure. As it is described in Table 1, when the concentration of Al in the synthesis gel is decreased, using SDAProp as OSDA, ZSM-5 is the crystallized phase. Therefore, it would be difficult to synthesize pure silica (or very low Al containing) ITQ-39 by working with low Al containing gels, unless we strongly favor crystallization of ITQ-39 with respect to ZSM-5. One way of doing that is by synthesizing a more selective OSDA. The potentially more selective OSDA has been rationalized as follows. A very adequate OSDA for the synthesis of pure silica ZSM-5 is tetrapropylammonium (TPA).[19] If SDAProp is

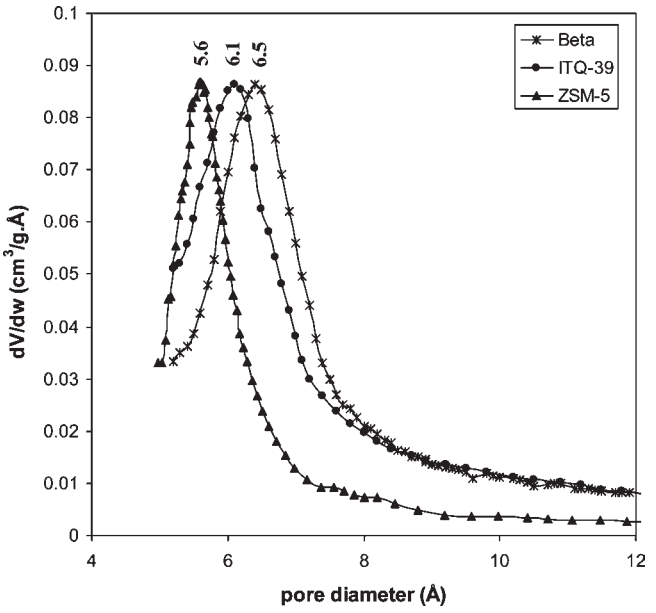

Figure 5. Pore distribution for Beta zeolite, ITQ-39, and ZSM-5 from Ar adsorption.

compared to TPA, it is clear that the former is larger but also presents high flexibility (as TPA), due to the presence of the propyl chains. Therefore, knowing the facility of TPA to form ZSM-5, and the capability of the SDAProp to direct the synthesis toward ZSM-5 when very small amounts of Al are present in the gel, we have reduced the flexibility of the OSDA in an attempt to avoid the nucleation of ZSM-5. To do that, the propyl groups introduced during the quaternization process (see Figure 1) have been replaced by methyl and ethyl groups.

The different phases obtained by using the SDAMet and SDAEt as OSDA are summarized in Table 4. It is noticeable that ZSM-5 is not crystallizing when the two less flexible OSDAs are used, validating the previous hypothesis. Furthermore, pure silica ITQ-39 was achieved after 14 days with the organic SDAEt.

dx.doi.org/10.1021/ja2015394 |J. Am. Chem. Soc. 2011, 133, 9497–9505

Table 4. Synthesis Conditions and Zeolites Obtained by Using SDAMet and SDAEt at Different Crystallization Times and T = 408 K

t (days)	Si/Al = 30	Si/Al = 50	Si/Al = ∞
		SDAMet	
7	amorphous	amorphous	amorphous
14	ITQ-39	ITQ-39	amorp-ITQ-39
21	ITQ-39	ITQ-39	amorp-dense phase-ITQ-39
		SDAEt	
7	amorphous	amorphous	amorp-ITQ-39
14	ITQ-39	ITQ-39	ITQ-39
21	ITQ-39	ITQ-39	ITQ-39

The elemental analysis of the as-prepared pure silica ITQ-39 confirms that the organic molecule precluded in the pores of the structure is intact, and the thermogravimetric analysis gives a weight loss of 23 wt %, similar to the aluminosilicate form of ITQ-39 (see Table 2).

When carrying out the synthesis in fluoride media, ^{19}F MAS NMR can give additional information about the presence in the structure of small cages, as secondary building units. For instance, ^{19}F MAS NMR has allowed one to identify the presence of F^- specifically inside small cages,[20] as for example the double-4-rings (D4R) in polymorph C of Beta zeolite (BEC), or $[4^35^4]$ cages in polymorphs A and B of Beta zeolite,[21] and the chemical shift in the ^{19}F MAS NMR spectrum depends on the cage where the fluoride anion is placed. In Figure 6, the ^{19}F MAS NMR spectrum of the as-prepared pure silica ITQ-39 zeolite shows four different signals. In the case of pure silica Beta zeolite, the ^{19}F MAS NMR spectrum gives two peaks at −59 and −70 ppm, assigned to fluoride anions in the $[4^35^4]$ cages of the polymorphs A and B.[21] Probably, the three bands observed in the case of ITQ-39 at −56.3, −61.4, and −70.8 ppm will be related to the presence of the cage $[4^35^4]$. However, the peak at −39.7 ppm is not shown in the spectrum of Beta zeolite, but it appears for pure silica BEC polymorph and has been associated to F^- into D4R cages.[22] Consequently, we can say that ITQ-39 zeolite framework shows characteristic small cages similar to those of the different polymorphs (A, B, and C) of the Beta family.

On other hand, the ^{29}Si MAS NMR spectrum shows the presence of, at least, four different atomic positions for the silicon atoms (see the bands between −108 and −120 ppm in Figure 7). However, those overlapped bands are broad due to the very small crystal size and the stacking disorder nature of the ITQ-39. Both observations support the presence of a large amount of structural defects in the zeolite framework, as is also indicated by the band in the ^{29}Si MAS NMR spectrum at −102 ppm (see Figure 7).

Up to now, with the results obtained from the different characterization techniques, we can say that ITQ-39 can be a three-dimensional zeolite with some structural characteristics close to those of Beta, but with a pore diameter and pore volume smaller than Beta and, more specifically, between those of Beta and ZSM-5. Now, we will attempt to obtain more detailed information about the pore topology of this zeolite by using test reactions in where the product distribution is a clear function of the zeolite pore structure. For doing that, we have considered as probe reactions the catalytic isomerization and disproportionation of xylenes and the alkylation of benzene and toluene with different alcohols. The above named reactions have shown clear utility to discern among medium and large pore zeolites the universus multidimensional pore structures, and the presence of lobes and channel crossing.[23]

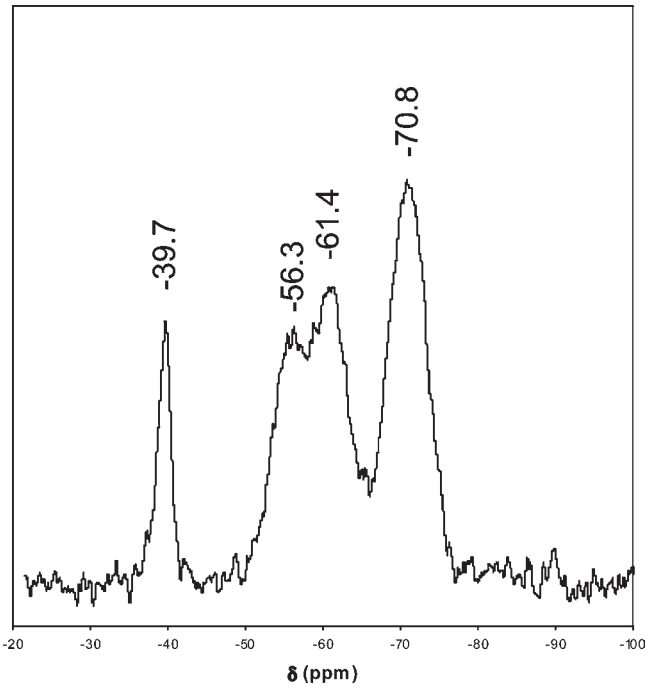

Figure 6. ^{19}F NMR spectrum for the as-prepared pure silica ITQ-39.

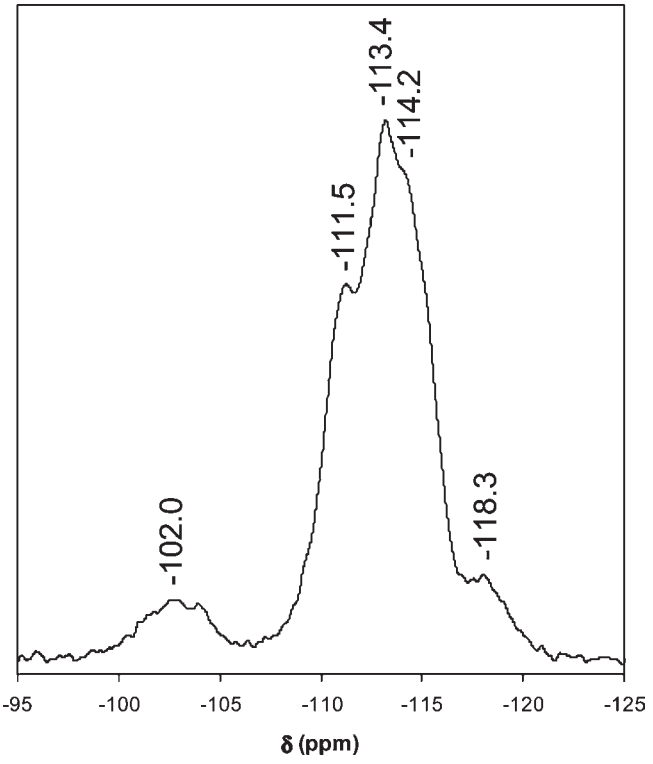

Figure 7. ^{29}Si NMR spectrum for the calcined pure silica ITQ-39.

Because all of the above are acid-catalyzed reactions, we have first studied the acid characteristics of ITQ-39 including the coordination of the Al present.

dx.doi.org/10.1021/ja2015394 |J. Am. Chem. Soc. 2011, 133, 9497–9505

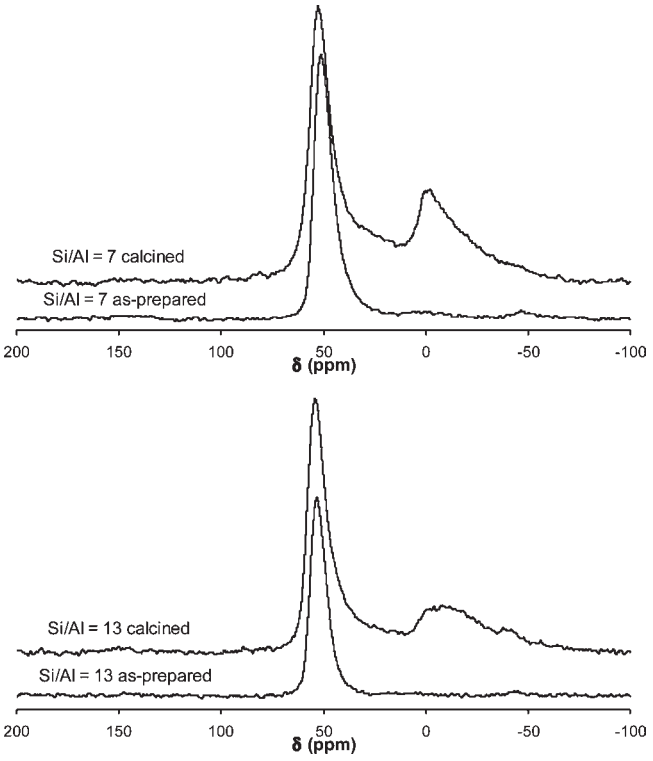

Figure 8. ^{27}Al NMR spectra for the as-prepared and calcined samples of ITQ-39 with Si/Al ratios of 7 and 13.

Table 5. Acid Properties of ITQ-39 Zeolite and Crystal Size in Comparison to Commercial Beta and ZSM-5 Samples

			acidity (adsorbance units)					
zeolite	crystal size (nm)	Si/Al_{real}	B423	B523	B623	L423	L523	L623
ZSM-5	200	11	356	351	293	63	61	60
Beta	170	13	159	110	49	386	371	325
ITQ-39		9.5	134	47	12	513	368	292
ITQ-39		11.5	111	47	9	433	308	250
ITQ-39	100−150	12.9	95	40	17	420	340	322
ITQ-39		22.1	74	50	24	365	344	330

As it has been shown in Table 1, ITQ-39 crystallizes in a broad Si/Al range. The Si/Al ratios in the crystalline materials are very similar to the theoretical values in the preparative gels (see Table 2). ^{27}Al MAS NMR experiments have been done with the as-synthesized samples with a Si/Al ratio of 6.7 and 13, and results from Figure 8 show a peak at ∼50 ppm that, as per its assignment, indicates that the aluminum is in tetrahedral coordination, and it mostly remains in tetrahedral coordination after calcination at 813 K. Furthermore, the study of pyridine adsorption−desorption by IR to determine acidity of those samples reveals the presence of pyridine being adsorbed as pyridinium ions even at desorption temperatures of 623 K in vacuum. Nevertheless, and for similar Si/Al ratio, both ZSM-5 and Beta give a larger number of acid sites retaining pyridine after desorption at 523 and 623 K, which can be assimilated in its behavior to acid sites with medium and strong acidity (see Table 5). We will see later that this difference in acidity has an important catalytic impact.

Table 6. Para/Ortho Ratio, Isomerization/Disproportionation Ratio, and Distribution of Trimethylbenzenes at Low Conversions of *meta*-Xylene on Different Zeolites at Atmospheric Pressure and 623 K

				trimethylbenzenes (normalized %)			
zeolite	X_0 (mol %)	*p*/*o*	i/d	1,3,5	1,2,4	1,2,3	1,2,3/1,3,5 ratio
ZSM-5	21.3	2.0	33.4		100.0		
	24.7	1.9	31.7		100.0		
ITQ-39	24.6	1.2	3.6	15.8	77.8	6.4	0.4
	26.5	1.3	3.1	16.1	76.8	6.3	0.4
	44.1	1.2	2.6	17.1	76.6	6.4	0.4
Beta	19.2	1.1	2.9	26.4	65.8	7.9	0.3
	34.8	1.1	2.3	27.3	64.4	8.3	0.3
equilibrium (623 K)		1.0		24.0	68.0	8.0	0.3

In the next section, the catalytic activity behavior and shape selectivity effects of ITQ-39 (sample with Si/Al = 13) will be compared to the large pore zeolite Beta (PQ13, Si/Al = 13) and the medium pore zeolite ZSM-5 (TZP322, Si/Al = 11).

3.2. Catalytic Experiments. *3.2.1. meta-Xylene Isomerization−Disproportionation.* As said before, the isomerization and disproportionation of *meta*-xylene allows differentiating between 10- and 12-MR pore zeolites, while indicating if there are lobes, cages, or crossing channels.[23] Both *para*- and *ortho*-xylenes are formed during the reaction at low levels of conversion, with the *para*/*ortho* ratios (*p*/*o*) being higher for 10-MR than for 12-MR pore zeolites, due to different rates of diffusion of the *para* and *ortho* isomers along the 10-MR channels. Moreover, the disproportionation of xylenes to give trimethylbenzenes and toluene is a bimolecular reaction that involves a bulkier reaction transition state than the monomolecular isomerization process. The ratio of isomerization to disproportionation (i/d) then will be an indicator of the presence of lobes, cavities, or crossing channels in where the available space could accommodate the bimolecular reaction. To this respect, the reactivity of ITQ-39 for *meta*-xylene gives a *p*/*o* ratio closer to Beta (see Table 6), indicating the presence, in the former, of 12-MR pores. However, when the i/d ratio is compared for the two large pore zeolites, there are significant differences. ITQ-39 always gives, at the same level of conversion, an i/d ratio higher than Beta and smaller than ZSM-5 (see Table 6). It is then apparent that while the 12-MR channels also cross in the case of ITQ-39, it must generate smaller void spaces within the structure than in the case of zeolite Beta, something that would also agree with the smaller micropore volume of the former zeolite (see Table 3). It is important to remark that in this case, the crystallite size of the two zeolites is quite similar, and, consequently, we cannot expect important differences in the ratio of external to internal surface and then on its impact on the i/d ratio (see Table 5).

Another parameter that can indicate the presence of internal cages, lobes, or crossing channels of different dimensions is the distribution of the trimethylbenzene (TMB) isomers formed by disproportionation of *meta*-xylene. The three isomers, that is, 1,2,4- 1,3,5-, and 1,2,3-TMB,[24] involve three different transition states. Those transition states cannot be easily accommodated into the pores of 10-MR zeolites, and when low amounts of disproportionation occur inside those channels, the less impeded complex (1,2,4-TMB) is the most favored. Thus, when the distribution of the trimethylbenzene isomers produced with

dx.doi.org/10.1021/ja2015394 |*J. Am. Chem. Soc.* 2011, 133, 9497–9505

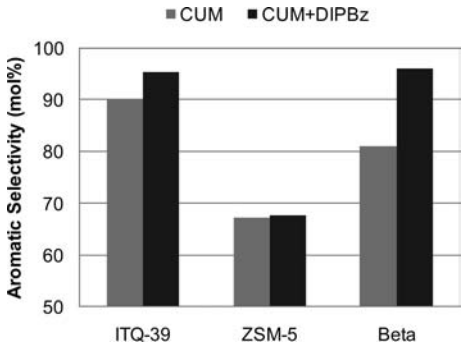

Figure 9. Aromatic selectivity of zeolites ITQ-39, ZSM-5, and Beta in benzene alkylation with isopropanol. Cumene (CUM), diisopropylbenzene (DIPB).

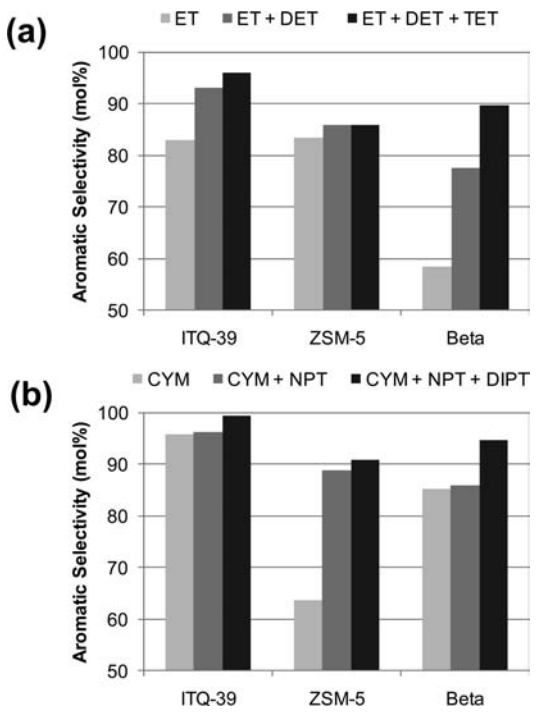

Figure 10. Aromatic selectivity of zeolites ITQ-39, ZSM-5, and Beta in toluene alkylation with ethanol (a) and isopropanol (b). Ethyltoluene (ET), diethyltoluene (DET), triethyltoluene (TET), cymene (CYM), *n*-propyltoluene (NPT), and diisopropyltoluene (DIPT).

zeolite ITQ-39 is compared to ZSM-5 and Beta, at several levels of *meta*-xylene conversion (see Table 6), it can be seen that 1,2,4-TMB is initially formed in a larger amount with ITQ-39 than with Beta but less than with ZSM-5. The analysis of these results indicates that the less bulky bimolecular transition state (1,2,4-TMB) is favored in the case of ITQ-39 with respect to Beta, in agreement with the possible presence of a three-directional large pore system with an effective pore diameter between that of Beta and ZSM-5 zeolite. A three-directional pore system with interconnected large and medium pores may also give the observed selectivity, although Ar adsorption was not able to show the presence of the two types of pores.

The 1,2,3-TMB/1,3,5-TMB ratio from initial selectivities obtained at low levels of disproportionation seems to reflect the shape of the pores. The 1,2,3-TMB/1,3,5-TMB ratio is then

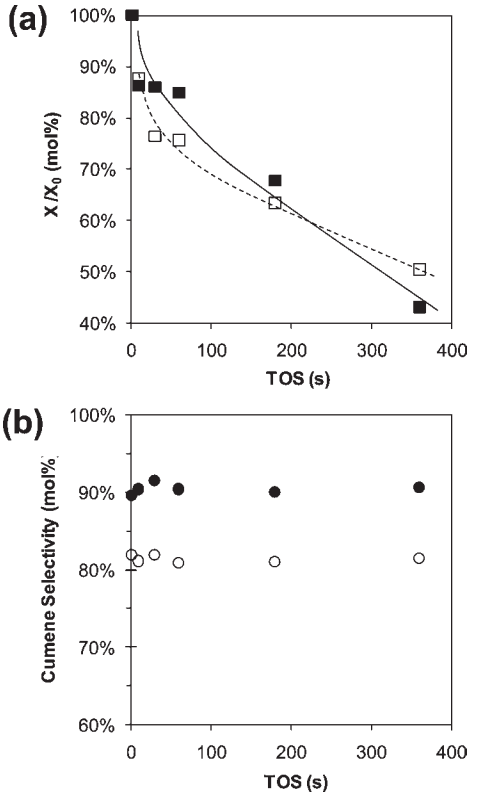

Figure 11. Time-on-stream behavior of ITQ-39 (filled) and Beta (empty) zeolites for benzene alkylation with isopropanol. (a) Conversion (■, □), (b) cumene selectivity (●, ○).

lower in zeolites with lobate pores (Y or L zeolites) than in zeolites where the configuration of the side pockets and side channels does not create regular lobes (Offretite, Mordenite, Omega).[23] In Table 6, one can see that the ratio of 1,2,3-TMB/1,3,5-TMB for ITQ-39 is higher than that for Beta zeolite, indicating that the reactants see smaller void spaces in the ITQ-39 than in Beta. As said before, the results are not masked by the reaction at the external surface because the crystallite size of the samples is very similar for ZSM-5, ITQ-39, and Beta (see Table 5).

3.2.2. Benzene and Toluene Alkylation. The alkylation of benzene or toluene with ethanol or propanol can be considered as an electrophilic substitution on the aromatic ring. When an alcohol is used as an alkylating agent, the isopropylation or ethylation reaction is believed to occur by the reaction of the activated alkene (formed by dehydration of the alcohol) on the acid sites of the zeolite. When the olefin is activated on the Brönsted acid site, it can react with benzene or toluene, mainly producing monoalkyltaed aromatics, polyalkylated aromatics, or *n*-propylalkylated aromatics, in the case of C_3^+ olefins or alcohols.

The conversion and the selectivities obtained for alkylation of benzene with isopropanol over ITQ-39, ZSM-5, and Beta zeolites are given in Table S1 in the Supporting Information. It can be seen there that ITQ-39 produces more cumene and less diisopropylbenzene than does Beta, which can be explained by the smaller voids within the structure of ITQ-39. The global selectivity to cumene plus diisopropylbenzene is higher for ITQ-39 than for the other samples (see Figure 9). Furthermore, the formation of the very undesired *n*-propylbenzene (NPB) is very

dx.doi.org/10.1021/ja2015394 |*J. Am. Chem. Soc.* 2011, 133, 9497–9505

low, and similar to Beta zeolite, as corresponds to a three-directional large pore zeolite.[25] This result can be of interest from an industrial point of view due to the high selectivity to cumene and low selectivity to NPB with ITQ-39. It is important to take into account, from an application point of view, that the level of oligomerization and olefins in the gas phase is smaller for ITQ-39 than either for ZSM-5 or for Beta. On the other hand, and despite the differences observed on acidity, the activity for benzene alkylation with isopropanol are similar (see Table S1 in the Supporting Information) for the three zeolites.

The catalytic results for toluene alkylation with ethanol are summarized in Table S2 in the Supporting Information. Interestingly, the aromatic selectivity to ethyltoluenes obtained is much higher for ITQ-39 than for Beta, with the sum of selectivities to ethylbenzene and the corresponding dialkylated products being also much larger with ITQ-39 (Figure 10a). The isopropylation of toluene follows the same tendency (see Table S3 in the Supporting Information and Figure 10b).

In general, the selectivity to monoalkylated products (ethyltoluene and cymene) is much larger for ITQ-39 than for Beta due to the large space restrictions existing in the former, which limit the formation and diffusion of the dialkylated and trialkylated products. Interestingly, the order of activity (see Table S2 in the Supporting Information) follows the order Beta > ITQ-39 > ZSM-5, which is the same than the pore dimensions.

When working under experimental conditions that lead to fast catalyst deactivation for benzene−isopropanol alkylation (see Figure 11), we can observe a similar deactivation rate for ITQ-39 and Beta, as it can be predicted by the oligomerization values obtained for both materials (see Table S1). Nevertheless, the selectivity to cumene is always larger with the new zeolite.

Taking into account the rate of cumene production, the selectivity to cumene, and the rate of catalyst deactivation, it appears to us that ITQ-39 is a highly promising environmentally friendly alkylation catalyst for manufacturing cumene by alkylation of benzene with propylene.

4. CONCLUSIONS

A new molecular sieve, named ITQ-39, has been synthesized. This zeolite shows an extensively faulted structure with very small domains that makes the structure elucidation very complicated. The characterization results by gas adsorption and spectroscopic studies indicate that this structure could be related to Beta zeolite, but with smaller pore diameter and lower pore volume. The use of test reactions, such as isomerization and disproportionation of *meta*-xylene, and benzene and toluene alkylation, added further information on pore topology, indicating that the unresolved ITQ-39 zeolite presents a three-directional channel system with large pores (12-MR), with an effective pore diameter and internal void spaces between that of Beta and ZSM-5 zeolite, or a three-directional channel system with interconnected large (12-MR) and medium pores (10-MR). The pore dimensions and topology of ITQ-39 result in very promising zeolite for its application to alkylation of aromatics with olefins.

■ ASSOCIATED CONTENT

Ⓢ Supporting Information. Tables containing the catalytic results of the benzene alkylation with isopropanol, toluene alkylation with ethanol, and toluene alkylation with isopropanol are summarized. This material is available free of charge via the Internet at http://pubs.acs.org.

■ AUTHOR INFORMATION

Corresponding Author
acorma@itq.upv.es

■ ACKNOWLEDGMENT

Financial support by the Spanish MICINN (MAT2009-14528-C02-01), Consolider Ingenio 2010-MULTICAT, Swedish Research Council (VR), the Swedish Governmental Agency for Innovation Systems (VINNOVA), and the Göran Gustafsson Foundation is gratefully acknowledged. Generalitat Valenciana is also thanked for funding through the Prometeo program. M.T.P. gratefully acknowledges CSIC for a JAE fellowship. The Knut and Alice Wallenberg Foundation for a grant for purchasing the TEMs used in this work is also thanked.

■ REFERENCES

(1) Corma, A. *J. Catal.* **2003**, *216*, 298.
(2) (a) Barrer, R. M.; Denny, P. J.; Flanigen, E. M. U.S. Patent 3306922, 1967. (b) Lobo, R. F.; Zones, S. I.; Davis, M. E. *J. Inclusion Phenom. Mol. Recognit. Chem.* **1995**, *21*, 47.
(3) Davis, M. E. *Nature* **2002**, *417*, 813.
(4) http://www.iza-online.org.
(5) (a) Sun, J. L.; Bonneau, C.; Cantín, A.; Corma, A.; Díaz-Cabañas, M. J.; Moliner, M.; Zhang, D.; Li, M.; Zou, X. D. *Nature* **2009**, *458*, 1154. (b) Corma, A.; Díaz-Cabañas, M. J.; Jiang, J.; Afeworki, M.; Dorset, D. L.; Soled, S. L.; Strohmaier, K. G. *Proc. Natl. Acad. Sci. U.S.A.* **2010**, *107*, 13997. (c) Corma, A.; Díaz-Cabañas, M. J.; Jorda, J. L.; Martinez, C.; Moliner, M. *Nature* **2006**, *443*, 842. (d) Jiang, J.; Jorda, J. L.; Diaz-Cabanas, M. J.; Yu, J.; Corma, A. *Angew. Chem., Int. Ed.* **2010**, *49*, 4986. (e) Tang, L. Q.; Shi, L.; Bonneau, B.; Sun, J. L.; Yue, H. J.; Ojuva, A.; Lee, B.-L.; Kritikos, M.; Zoltán, B.; Mink, J.; Bell, R. G.; Zou, X. D. *Nat. Mater.* **2008**, *7*, 381.
(6) (a) Song, X.; Li, Y.; Gan, L.; Wang, Z.; Yu, J.; Xu, R. *Angew. Chem., Int. Ed.* **2009**, *48*, 314. (b) Yu, J.; Xu, R. *Acc. Chem. Res.* **2010**, *43*, 1195.
(7) McCusker, L. B.; Baerlocher, Ch. *Stud. Surf. Sci. Catal.* **2008**, *174A*, 13.
(8) Wadlinger, R. L.; Kerr, G. T.; Rosinski, E. J. U.S. Patent 3308069, 1967, Mobil Oil Corp.
(9) Treacy, M. M. J.; Newsam, J. M. *Nature* **1988**, *332*, 249.
(10) Newsam, J. M.; Treacy, M. M. J.; Koetsler, W. T.; deGruyter, C. B. *Proc. R. Soc. London, Ser. A* **1988**, *420*, 375.
(11) (a) Gramm, F.; Baerlocher, Ch.; McCusker, L. B.; Warrender, S. J.; Wright, P. A.; Han, B.; Hong, S. B.; Liu, Z.; Ohsuna, T.; Terasaki, O. *Nature* **2006**, *444*, 79. (b) Baerlocher, Ch.; Gramm, F.; Massüger, L.; McCusker, L. B.; He, Z. B.; Hovmöller, S.; Zou, X. D. *Science* **2007**, *315*, 1113. (c) Baerlocher, Ch.; Xie, D.; McCusker, L. B.; Hwang, S.-J.; Chan, I. Y.; Ong, K.; Burton, A. W.; Zones, S. I. *Nat. Mater.* **2008**, *7*, 631.
(12) (a) Corma, A.; Moliner, M.; Cantín, A.; Díaz-Cabañas, M. J.; Jordá, J. L.; Zhang, D. L.; Sun, J. L.; Jansson, K.; Hovmöller, S.; Zou, X. D. *Chem. Mater.* **2008**, *20*, 3218. (b) Sun, J. L.; He, Z. B.; Hovmoller, S.; Zou, X. D.; Gramm, F.; Baerlocher, C.; McCusker, L. B. *Z. Kristallogr.* **2010**, *225*, 77.
(13) Corma, A.; Moliner, M.; Rey, F.; González, J. WO2008/092984 A1, 2008.
(14) Corma, A.; Chica, A.; Guil, J. M.; Llopis, F. J.; Mabilon, G.; Perdigon-Melon, J. A.; Valencia, S. *J. Catal.* **2000**, *189*, 382.
(15) (a) Corma, A.; Costa-Vaya, V. L.; Díaz-Cabañas, M. J.; Llopis, F. J. *J. Catal.* **2002**, *207*, 46. (b) Zilkova, N.; Bejblova, B.; Gil, B.; Zones, S. I.; Burton, A. W.; Chen, C. Y.; Musilova-Pavlackova, Z.; Kosovo, G.; Cejka, J. *J. Catal.* **2009**, *226*, 79.

(16) Zou, X. D.; Sukharev, Y.; Hovmöller, S. *Ultramicroscopy* **1993**, *49*, 147.
(17) Horvath, G.; Kawazoe, K. *J. Chem. Eng. Jpn.* **1983**, *16*, 470.
(18) Simancas, R.; Dari, D.; Velamazán, N.; Navarro, M. T.; Cantin, A.; Jorda, J. L.; Sastre, G.; Corma, A.; Rey, F. *Science* **2010**, *330*, 1219.
(19) Burkett, S. L.; Davis, M. E. *Chem. Mater.* **1995**, *7*, 920.
(20) Fyfe, C. A.; Brouwer, D. H.; Lewis, A. R.; Villaescusa, L. A.; Morris, R. E. *J. Am. Chem. Soc.* **2002**, *124*, 7770.
(21) Vidal-Moya, J. A.; Blasco, T.; Corma, A.; Navarro, M. T.; Rey, F. *Stud. Surf. Sci. Catal.* **2004**, *154*, 1289.
(22) Cantin, A.; Corma, A.; Diaz-Cabañas, M. J.; Jorda, J. L.; Moliner, M.; Rey, F. *Angew. Chem., Int. Ed.* **2006**, *45*, 8013.
(23) (a) Csicsery, S. M. *Zeolites* **1984**, *4*, 202. (b) Olson, D. H.; Haag, W. O. *ACS Symp. Ser.* **1984**, *248*, 275. (c) Martens, J. A.; Perez-Pariente, J.; Sastre, E.; Corma, A.; Jacobs, P. A. *Appl. Catal.* **1988**, *45*, 85. (d) Zones, S. I.; Chen, C. Y.; Corma, A.; Cheng, M.; Kibby, C. L.; Chan, I. Y.; Burton, A. W. *J. Catal.* **2007**, *250*, 41.
(24) Llopis, F. J; Sastre, G.; Corma, A. *J. Catal.* **2006**, *242*, 195.
(25) Corma, A.; Martínez-Soria, V.; Schnoeveld, E. *J. Catal.* **2000**, *192*, 163.